Langmuir

Article

pubs.acs.org/Langmuir

Self-Assembly of a Designed Alternating Arginine/Phenylalanine Oligopeptide

Carla C. Decandio,[†] Emerson R. Silva,*[,†,‡] Ian W. Hamley,[‡] Valeria Castelletto,[‡] Michelle S. Liberato,[†] Vani X. Oliveira, Jr.,[†] Cristiano L. P. Oliveira,[§] and Wendel A. Alves*[,†]

[†]Centro de Ciências Naturais e Humanas, Universidade Federal do ABC, Santo André 09210-580, Brazil

[‡]Department of Chemistry, University of Reading, Whiteknights, Reading RG6 6AD, United Kingdom

[§]Instituto de Física, Universidade de São Paulo, São Paulo 05314970, Brazil

Supporting Information

ABSTRACT: A model octapeptide peptide consisting of an alternating sequence of arginine (Arg) and phenylalanine (Phe) residues, namely, [Arg-Phe]$_4$, was prepared, and its self-assembly in solution studied. The simple alternating [Arg-Phe]$_4$ peptide sequence allows for unique insights into the aggregation process and the structure of the self-assembled motifs. Fluorescence and UV−vis assays were used to determine critical aggregation concentrations, corresponding to the formation of oligomeric species and β-sheet rich structures organized into both spheroidal aggregates and highly ordered fibrils. Electron and atomic force microscopy images show globular aggregates and long unbranched fibers with diameters ranging from ∼4 nm up to ∼40 nm. Infrared and circular dichroism spectroscopy show the formation of β-sheet structures. X-ray diffraction on oriented stalks show that the peptide fibers have an internal lamellar structure, with an orthorhombic unit cell with parameters $a \sim 27.6$ Å, $b \sim 9.7$ Å, and $c \sim 9.6$ Å. In situ small-angle X-ray scattering (SAXS) shows the presence of low molecular weight oligomers in equilibrium with mature fibers which are likely made up from 5 or 6 intertwined protofilaments. Finally, weak gel solutions are probed under gentle shear, suggesting the ability of these arginine-rich fibers to form networks.

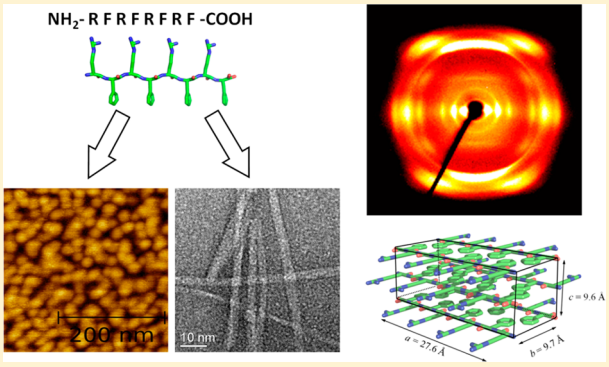

INTRODUCTION

The fibrillization of peptides has attracted a lot of interest due to its close association with degenerative diseases such as Alzheimer's, Parkinson's, and diabetes type II.[1−4] It is widely recognized that such disorders arise from protein misfolding followed by self-assembly into cytotoxic oligomers which form fibrillar structures, usually rich in β-strands, which are so-called amyloid fibrils.[5] Within this context, understanding the mechanisms involved in amyloid formation is a significant challenge from the point-of-view of fundamental research or from the perspective of control and treatment of these diseases.

Despite the fact that the formation of amyloid fibrils is typically observed for relatively large proteins, it has been shown that fibrillization is possible for short sequences presenting specific residues.[6−8] For example, Tjernberg and co-workers studied fibril formation from short segments derived from the Alzheimer's peptide Aβ-40[6,7,9−11] containing from 3 to 10 amino acids. The self-assembly into amyloid fibers was observed only for sequences containing more than five residues, all the sequences containing phenylalanine residues. Since then, phenylalanine and its strong ability for π-stacking interactions have been thought to play a major role in amyloid formation.[12] Thus, understanding the fibrillization of short peptides containing aromatic residues, such as phenylalanine, provides a close insight into the formation of amyloid-like structures. Unfortunately, a detailed framework to explain amyloid formation is still lacking, although some general aspects are well-established and appear to be shared among different amyloid fibers. For instance, morphological assays systematically show that amyloid fibers are ∼10 nm wide and a few micrometers long. The internal structure of amyloid fibers consists of antiparallel β-strands self-organized into β-sheets which run parallel to the long axis of the fibrils. The final structures appear as a result of the stacking of protofilaments into mature fibers.[5,13,14]

Herein, we investigate the aggregation behavior of a model octapeptide, containing L-phenylalanine (Phe) and L-arginine (Arg) residues in the sequence [Arg-Phe]$_4$.[15] The generic sequence consisting of intercalated hydrophilic and hydrophobic amino acids, corresponds to a Type I peptide of the "molecular Lego" group, a family of peptides with recognized capabilities to form fibrillar assemblies usually rich in β-sheet

Received: January 21, 2015
Revised: March 12, 2015
Published: March 30, 2015

DOI: 10.1021/acs.langmuir.5b00253
Langmuir 2015, 31, 4513−4523

structures.[16,17] In addition, octapeptides have been successfully used to form fibers and to prepare hydrogel matrices with potential biotechnological applications.[18−21] Our purpose here is to provide detailed information on the aggregation and structure of $[Arg\text{-}Phe]_4$, which is rich in arginine and does not rely on complementary ionic pairing for the self-assembly.[16] The choice of Arg and Phe is motivated by the properties of their side-chains. Phe presents an aromatic side chain able to establish strong $\pi-\pi$ interactions and promote amyloid fiber formation.[8,11] Arg is endowed with a side-chain guanidinium group, making it a strong H-bond donator.[22] Arg is positively charged at physiological pH, enabling cation$-\pi$ interaction between the NH^+ group and the phenyl ring in the Phe side-chain.[23] The self-assembly of $[Arg\text{-}Phe]_4$ into fibers, using a solid−vapor deposition strategy, was previously reported by us.[15] Here, we report a detailed study of $[Arg\text{-}Phe]_4$ self-assembly in solution by using a wide range of experimental techniques encompassing spectroscopy, microscopy, and X-ray methods to determine the critical aggregation concentration. We characterize in detail the secondary structure and give insights into the pathway leading to the formation of fibers. We show that this simple alternating cationic octapeptide exhibits many features of amyloid-fibrils and is a potential model for investigating fibrillization.

EXPERIMENTAL SECTION

Peptide Synthesis. All chemicals had analytical or HPLC grade. Protected amino acids, [(Boc-Phe-OH)] and [(Boc-Arg(Tos)-OH)], 1,3-diisopropylcarbodiimide/*N*-hydroxybenzotriazole (DIC/HOBt), trifluoroacetic acid (TFA), anisole, dichloromethane (DCM), dimethylformamide (DMF), diisopropylethylamine (DIEA), and acetonitrile (ACN) were purchased from Sigma-Aldrich (Saint Louis, MO). Chloromethyl resin (Merrifield) was purchased from Advanced Chemtech (Louisville, KY), with substitution degree 0.90 mmol/g and starting amino acid coupled to the polymeric support. The synthesis of the octapeptides was performed as detailed elsewhere,[15] and, in brief, the procedure was as follows: the protected group was removed by reaction with 50% TFA and 2% anisole in DCM for 20 min. Coupling was carried out in 2.5 fold excess of DIC/HOBt in DCM/DMF (1:1, v:v). Reactions were monitored using the Kaiser ninhydrin test and peptidyl resin was acetylated with 25% acetic anhydride in DMF with excess DIEA for 20 min. Dry-protected resin was exposed to 70% TFA + 20% TFMSA and 10% anisole during 12 h, at 4 °C. After free-drying, crude peptide was purified by reverse-phase HPLC in aqueous solutions of ACN + 0.1% TFA (60:40, v:v) on a Waters Delta Prep 600 system, exhibiting purity > 96%. Mass spectrometry was conducted on a liquid-chromatography electrospray-ionization mass spectrometer, LC/ESI-MS, yielding $[Arg\text{-}Phe]_4$ (MM + H) = 1276 (calculated = 1275).

Sample Preparation. Aqueous solutions were prepared by dissolving peptides in Milli-Q water (resistivity > 18 MΩ·cm at 25 °C), at concentrations typically ranging from 1×10^{-5} to 2 wt %. Measurements with indicator paper showed pH between ∼6.0 (at higher peptide concentrations) and ∼7.5 across the investigated range. For Fourier transform infrared (FTIR) experiments, solutions were prepared in D_2O (Fluka). Critical aggregation concentration measurements were performed using solutions containing thioflavin T (ThT) at 1×10^{-3} wt %, pyrene (Pyr) or 1-pyrenecarboxylic acid (1PCA) at 1×10^{-4} wt %. Samples were submitted to ultrasound just after mixing (50 °C, ∼15 min) and then stored in the dark to equilibrate at room temperature for at least 24 h before further analyses.

Spectroscopy Methods. Fluorescence spectra were recorded on a PerkinElmer spectrometer. Samples were loaded into a 10 mm inner width quartz cuvette. Excitation wavelengths were λ_{ex} = 338 nm or λ_{ex} = 440 nm for solutions containing Pyrene or ThT, respectively. Excitation and emission slits were kept at 5 nm and spectra were recorded in the (345−500) nm or (450−600) nm range for Pyr and ThT fluorescence assays, respectively. Absorbance profiles were monitored on a Varian Cary 50 spectrophotometer. Solutions were loaded into a 10 mm path length quartz cuvette. The UV−vis range was scanned from 220 to 370 nm and the data was treated for baseline correction. FTIR assays were carried out on a Varian 660-IR spectrometer operating in ATR mode. Droplets from $[Arg\text{-}Phe]_4$ solutions in D_2O were deposited onto a ZnSe crystal and left to dry, and 80 accumulations were obtained in the interval 1500−1800 cm^{-1}, with step resolution of 2 cm^{-1}. After background subtraction, resonances were deconvoluted and fitted to Gaussian profiles using the program *Fityk*[24] to enable accurate assignment. Circular dichroism (CD) measurements were performed using synchrotron radiation at the CD beamline B23 (Diamond Light Source, U.K.), using the nitrogen-flushed Module B end-station spectrophotometer. The samples were loaded in CaF_2 cells with path lengths varying between 0.05 and 10 mm according to concentration in order to optimize absorbance. Data have been converted into mean residue ellipticity units (MRE) for comparison between different concentrations and path lengths. The data, recorded with a 1 nm step and 1 s collection time per step, are presented as the averaged results from four scans. CD data was corrected by background from the solvent, and correspond to absorbance $A < 2$ at any measured point. All experiments were performed at 20 °C.

Microscopy Imaging. Atomic force microscopy (AFM) and high-resolution transmission electron microscopy (HRTEM) were carried out at the Brazilian Nanotechnology National Laboratory (Campinas, Brazil). AFM was performed using a Digital Instruments Nanoscope III operating in tapping mode. Droplets were deposited onto freshly cleaved mica substrates, left to rest for a couple of minutes, rinsed with deionized water, and dried overnight under a gentle nitrogen stream. Images were obtained by scanning 1024 × 1024 pixels covering surfaces between 1 and 5 μm^2. Topology and phase data were enhanced and analyzed using the *Gwydion* package.[25] Electron microscopy was performed on a TEM-HR JEOL 3010 instrument operating at 300 kV. Drops from a peptide solution were cast onto Cu grids coated with carbon film, stained with a 2% uranyl acetate solution (Sigma), and allowed to dry in a desiccator.

Fiber Diffraction and Small-Angle X-ray Scattering. Fiber diffraction patterns were recorded from oriented stalks obtained by suspending droplets of a 5 wt % peptide solution between the ends of wax-coated capillaries and letting them dry in air at room temperature (RT). We observed that solutions incubated for at least 10 days at RT were much better able to produce well-oriented samples. Stalks were vertically positioned onto a RAXIS IV++X-ray diffractometer (Rigaku) equipped with a rotating anode generator, and data were collected using a Saturn 992 CCD camera, with sample-to-detector distance of 40 mm. Small-angle X-ray scattering (SAXS) was carried out on the BioSAXS BM29 beamline at the ESRF (Grenoble, France). Solutions were loaded into PCR tubes in an automated sample changer kept at 20 °C. Around 50 μL from solutions was injected into a 1 mm quartz capillary, and successive frames of 0.2 s each were registered during flow to avoid radiation damage. Data were recorded using a Pilatus 1 M detector, positioned at sample-to-detector distance of 2864 mm. The X-ray wavelength was λ = 0.99 Å and reduction to 1D intensity curves was performed by radial integration using the beamline software. This configuration provided high-resolution data in the range 0.04 $nm^{-1} \leq q \leq$ 4.9 nm^{-1} (where $q = 4\pi/\lambda \sin\theta$, with 2θ being the scattering angle). Fit2D was used to process 2D images from both X-ray diffraction (XRD) and SAXS assays. The program CLEARER[26] was used for optimizing unit cell parameters from XRD assays, and the SASFit package[27] was used to fit all scattering data.

RESULTS AND DISCUSSION

Critical Aggregation Concentrations. Fluorescence experiments were used to determine the critical aggregation concentration (cac) of $[Arg\text{-}Phe]_4$. The cac was measured in three separate experiments, by preparing a series of peptide solutions using Pyr, ThT, or 1PCA as a probe. In these experiments, the concentration of fluorophore (probe) was

DOI: 10.1021/acs.langmuir.5b00253
Langmuir 2015, 31, 4513−4523

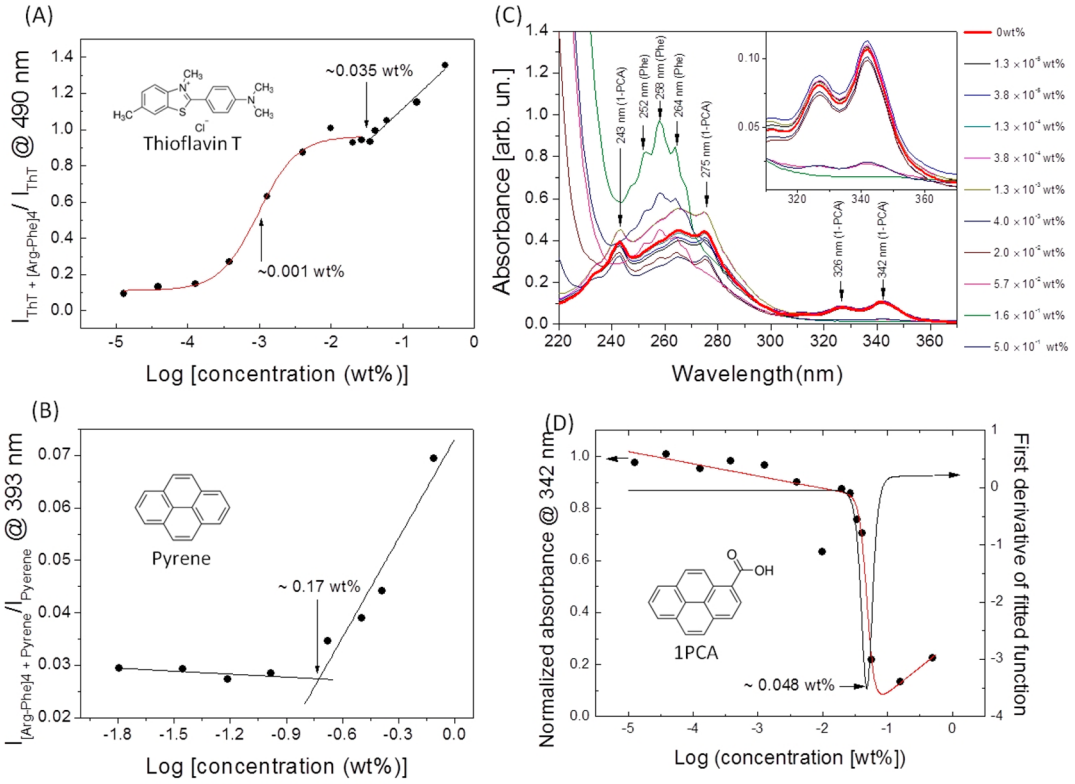

Figure 1. Estimation on critical concentrations from spectroscopy assays. (A) Behavior of ThT fluorescence as a function of log[concentration] in solution containing the probe at 1×10^{-3} wt %. Red line is a sigmoidal fit, and black line is a linear fit. (B) Pyrene fluorescence from solutions containing the probe at 1×10^{-5} wt %. (C) Absorbance profiles of 1PCA in solutions containing [Arg-Phe]4 at different concentrations. Inset: 1-PCA resonances used to probe the cac. (D) Intensity of band at 342 nm as a function of log[concentration]. Data were fitted by a modified sigmoid function (red line), and cac obtained from the minimum of the first derivative (gray line).

kept constant whereas the amount of peptide was varied across a wide concentration range. ThT has been widely used to identify and quantify amyloid structures due to the enhancement of its fluorescence emission upon association to β-sheet assemblies.[5,28,29] The exact mechanisms involved in this process is not fully understood. However, it has been suggested that intercalation of the ThT probe into β-sheet grooves suppresses torsions and twists of the ThT, favoring higher fluorescence yields.[28] Pyr species, in turn, are hydrophobic compounds, highly sensitive to the polarity of the medium.[30,31] During the self-assembly of peptide monomers in a Pyr solution, the Pyr is sequestered within the self-assembled hydrophobic clusters and the fluorescence of the probe is enhanced. The 1PCA chromophore is very similar to Pyr, but it possesses a carboxyl group attached to the pyrenyl moiety (see insets in Figure 1). This polar group gives a slightly amphiphilic behavior to the probe, modifying its interaction with the assemblies in solution. Since our $[Arg\text{-}Phe]_4$ peptide contains alternating polar and nonpolar amino acids, 1PCA is able to interact with either hydrophilic or hydrophobic sites in the arrays. Therefore, we have monitored characteristic bands in the absorbance profile to estimate the cac. The use of three different probes, that is, ThT, Pyr, and 1PCA, provides measurements based on independent mechanisms allowing for estimations of cac values of intermediate species on the self-assembly pathway.

In Figure 1A, we show the dependence of ThT fluorescence as a function of the peptide concentration. Emission was measured at $\lambda_{em.}$ = 490 nm (maximum) and data were normalized to the intensity found in a peptide-free solution. The curve exhibits two distinct concentration regimes. The more dilute domain is characterized by normalized fluorescence intensities below unity, indicating a possible quenching of chromophore in solution. In the second domain, the emission exhibits a plateau followed by a linear fluorescence increase which is assigned to appearance of β-sheet-rich structures.[5] To provide a quantitative estimation of the cac arising from these two regimes, we have fitted the data at the low-concentration regime using a sigmoidal function characterized by an inflection point at 0.0010 ± 0.0005 wt % peptide. This value is taken as an estimation of critical concentration and could be associated with formation of low molecular weight oligomers without well-organized structures. The second domain has been fitted with a linear function and its intercept with the plateau has been found at 0.035 ± 0.010 wt % peptide.

Figure 1B shows the intensity of the fluorescence emission of Pyr as a function of the peptide concentration. Fluorescence was monitored at the emission maximum, λ_{em} = 393 nm. The Pyr fluorescence emission in solutions containing peptide is much lower than in peptide-free solutions, across the entire peptide concentration range. This finding results from the unique design of $[Arg\text{-}Phe]_4$, which contains an equal number of phenyl and guanidium moieties alternating along the sequence. In this case, Pyr species interacting with phenyl groups in the assemblies are also surrounded by strongly polar Arg side-chains hindering an appreciable growth of fluorescence. Also, at neutral pH, Arg residues are positively charged and this likely implies very high ionic strength in medium. Despite the complex interplay between electrostatic and aromatic stacking interactions, it is possible identify a clear inflection point at 0.17 ± 0.03 wt % peptide (Figure 1B) which

DOI: 10.1021/acs.langmuir.5b00253
Langmuir 2015, 31, 4513−4523

is attributed to the appearance of a higher level of organization, maybe with polar and nonpolar galleries spatially separated within the assemblies. As discussed below, this critical concentration could be attributed to formation of fibers in solution exhibiting a well-defined crystalline ordering.

Figure 1C shows the UV−visible spectra measured for peptide solutions containing 1PCA. The absorbance patterns in Figure 1C are quite complex, exhibiting resonances that arise either from 1PCA or from the aromatic groups at the Phe side-chains. In addition, the profiles depend on the concentration of peptide, with the appearance and disappearance of resonances across the UV−vis range. Again, two regimes are observed. In the more diluted one, spectra are dominated by four strong peaks at 243, 275, 326, and 342 nm. These resonances are characteristic of 1PCA and have been assigned to $\pi-\pi^*$ transitions in the molecule.[32] As the amount of $[\text{Arg-Phe}]_4$ increases, a systematic decrease in intensity of these bands is observed and the effect is even more remarkable in the near UV-region, where a doublet at 326 and 342 nm is found (see insert in Figure 1C). Along with the disappearance of 1PCA bands, three peaks characteristic of phenylalanine-containing compounds, emerge at 252 nm, 258 and 264 nm.[33] To estimate the cac, we have normalized the 1PCA peak at 342 nm to the intensity measured in a peptide-free solution and plotted the resulting values as a function of peptide concentration (see Figure 1D). The curve has a sigmoid-like shape with an abrupt transition between the domains reported above. To properly describe this sudden changeover, we have used an empirical function which has been successfully employed in titration assays to describe the behavior of enthalpy changes close to the critical micelle concentration.[34,35]

$$I_{\text{abs}} = \frac{a_1[\log(c)] + a_2}{1 + \exp\left(\frac{[\log(c)] - a_3}{\Delta_{a_3}}\right)} + a_4[\log(c)] + a_5 \quad (1)$$

In eq 1, I_{abs} is the normalized absorbance and c is the peptide concentration. Parameters a_1 and a_4 are the slope while a_2 and a_5 are the intercept terms to account for the linear regions of the profiles. Parameters a_3 and Δ_{a_3} are the parameters of an exponential profile used to describe a transition between regimes, and correspond to the inflection point of the curve (a_3) and the width (Δ_{a_3}) of the transition. The cac was determined as the minimum of the first derivative of the fitted curve in Figure 1D, while the corresponding FWMH (full width at half-maximum) was taken as the uncertainty, providing cac ∼ 0.048 ± 0.011 wt % peptide. Since this value is in good agreement with the cac found from the ThT (Figure 1A), the transition point in Figure 1D was attributed to the formation of β-sheet structures in solution.

Gathering the results exhibited above, we conclude that the aggregation behavior is complex and different levels of organization likely appear along the self-assembly pathway. Briefly, the results in Figure 1 provide three critical concentrations: cac_1 = 0.001 ± 0.005 wt % peptide, cac_2 = 0.042 ± 0.017 wt % peptide and cac_3 = 0.17 ± 0.03 wt % peptide. Accurate interpretations of these critical points are not trivial; however, on the basis of data presented in the following, we can tentatively assign them, respectively, to oligomeric species (cac_1), formation of globular aggregates (cac_2) containing β-sheet cores and, finally, the appearance of amyloid-fibers in solution (cac_3).

Secondary Structure. The secondary structure of the self-assembled peptide was investigated performing FTIR and CD experiments. Figure 2A shows a representative FTIR spectrum

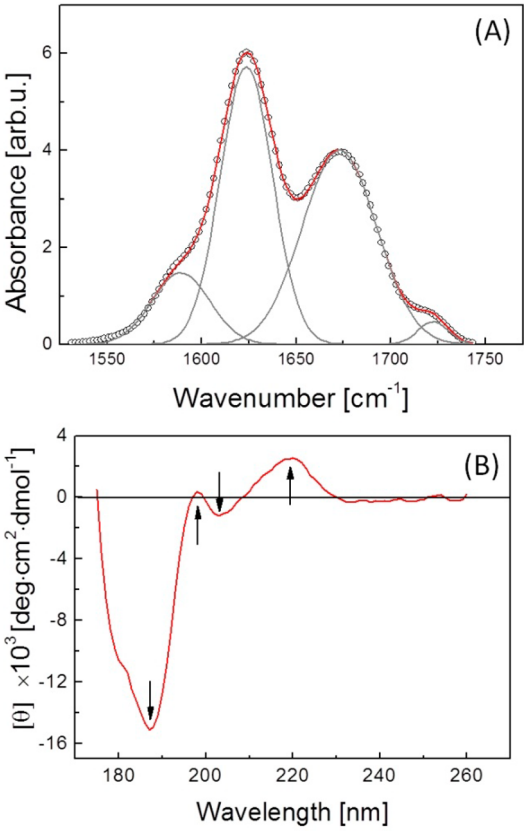

Figure 2. Secondary structure assays. (A) FTIR data of a 0.25 wt % $[\text{Arg-Phe}]_4$ solution into D_2O. Gray lines correspond to deconvoluted bands with peaks at 1589, 1624, 1673, and 1722 cm^{-1}. (B) CD spectrum from a sample at 0.05 wt % into H_2O.

corresponding to 0.25 wt % $[\text{Arg-Phe}]_4$ in D_2O, above cac_3 and presumably containing fibers in solution. We have focused our analyses on the amide I region, where vibrations from C═O stretching provide information about the backbone conformation.[36] Deconvolution using Gaussian peak fitting reveals that the amide I region is dominated by a pronounced peak at 1624 cm^{-1}, corresponding to a classical signature of β-sheets formed via H-bonds between adjacent strands.[5] The observed narrow and strong peak is consistent with highly delocalized vibrational modes oriented along the axis perpendicular to strands and points to a high level of organization presumably into a cross-β structure.[37] A second strong peak is observed at 1673 cm^{-1} and it is assigned to the presence of TFA counterions in solution.[38] These vibrations appear flanked by two shallow shoulders at 1589 and 1722 cm^{-1}. The resonance at 1589 cm^{-1} may be attributed to modes within arginine side-chains[39,40] and the mode at 1722 cm^{-1} is assigned to H-bonded carboxylic acid stretch,[41] indicating an acidic environment in agreement with the presence of TFA in solution.

Investigating secondary structure at lower concentrations via FTIR methods is a nontrivial task because of sensitivity limitations. In this case, CD analysis could be an alternative tool to probe the secondary structure.[42] A representative CD spectrum from $[\text{Arg-Phe}]_4$ solutions is exhibited in Figure 2B and supplementary data are found in Supporting Information

DOI: 10.1021/acs.langmuir.5b00253
Langmuir 2015, 31, 4513−4523

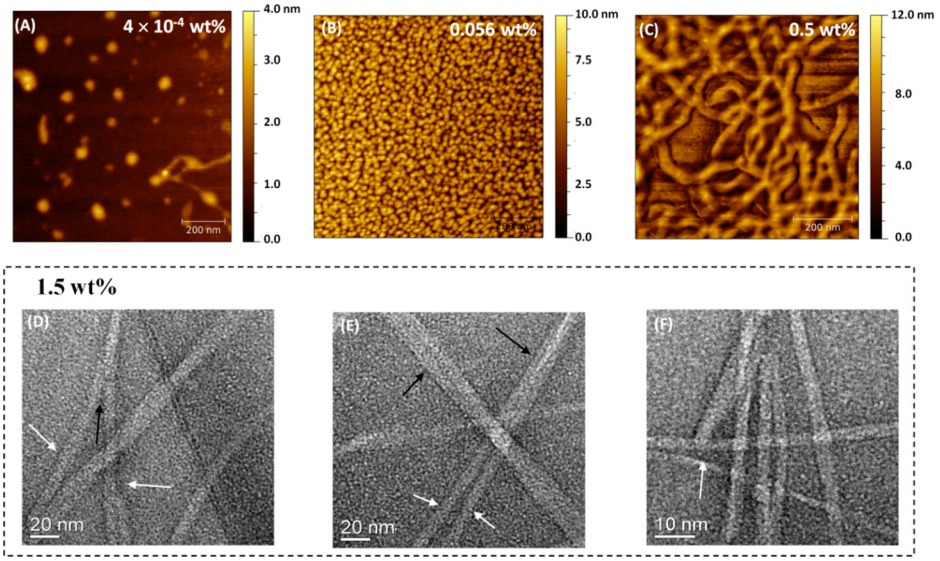

Figure 3. Top row: Ex situ AFM imaging from $[Arg\text{-}Phe]_4$ solutions at different concentrations, 4×10^{-4} wt %, below cac_1; 0.056 wt %, marginally above cac_2; and 0.5 wt %, well above cac_3. Bottom row: HRTEM images from a 24 h old sample at 1.5 wt %. (D, E) White arrows point to smaller fibrils which form wider intertwined fibers (indicated by black arrows). (F) Arrow points to the lowest fibril observed in our images, only ~2.0 nm wide. Also, in the middle of the image, it is possible visualize twisted fibrils.

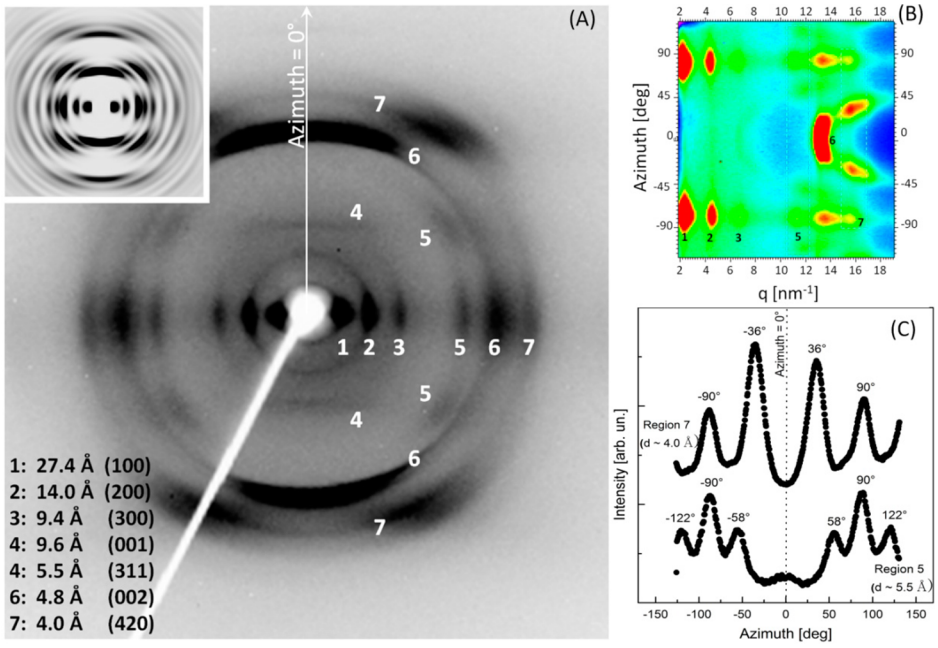

Figure 4. (A) XRD pattern from an oriented stalk dried from a 5 wt % $[Arg\text{-}Phe]_4$ solution showing the respective indexation. Inset: Simulated fiber diffraction pattern arising from an orthorhombic unit cell with a = 27.6 Å, b = 9.7 Å, and c = 9.6 Å. (B) Polar representation of pattern exhibited in (A). Data are shown between ±135° to avoid overlap with beam stopper. (C) azimuthal profiles of q-integrated intensities in thin coronas centered around off-axis peaks (white dashed rectangles in (B)).

Figure SI_1. The extensive presence of aromatic chromophores (50% of our peptide are made of Phe residues) leads to heavily mixed spectra exhibiting electronic transitions from peptide backbones and/or benzene side-chains.[43,44] In this case, it is not possible to provide unequivocal assignments exclusively on the basis of CD spectroscopy and only qualitative analysis has been made by comparing our data with fluorescence or FTIR information. As a rule, the spectra for the octapeptide systematically exhibit a pronounced negative band at 188 nm, followed by a shallow positive maximum at 198 nm. This signature has been previous assigned to β-turns and β-pleated sheet conformations.[45] At higher wavelength, a weak minimum is observed at 203 nm and a intense positive maximum emerges at 219 nm. The shallow negative band could be related to a small fraction of disordered secondary structures,[43] whereas the strong positive peak arises from $n-\pi^*$ transitions within the phenyl groups in phenylalanine.[42−44] In samples with concentrations above cac_2, the growth in ThT emission observed in Figure 1A also suggests the presence of β-sheet cores in these aggregates. For concentrations above cac_3, FTIR spectra shown in Figure 2A and XRD data discussed below unequivocally show β-sheet organization.

DOI: 10.1021/acs.langmuir.5b00253
Langmuir 2015, 31, 4513−4523

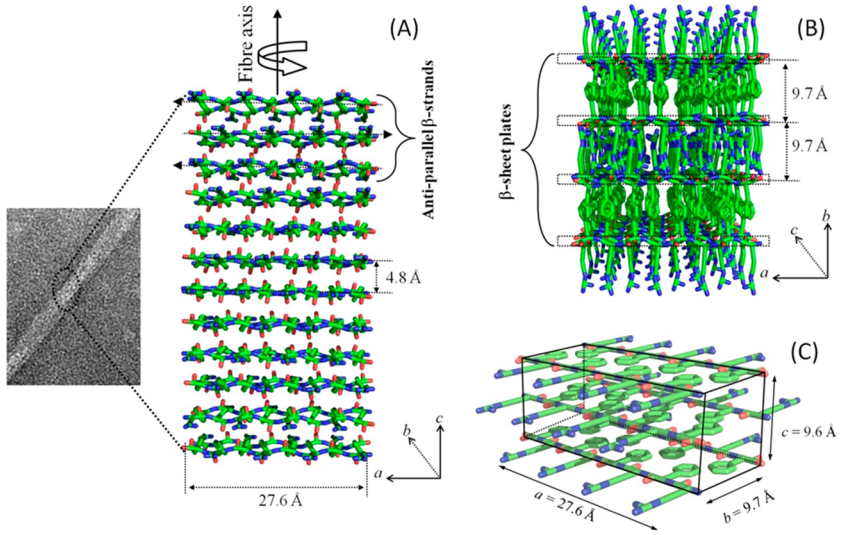

Figure 5. Scheme of structure based on XRD data. Perspective views highlight the stack of antiparallel cross-β chains formed along the fiber axis (A) and organization into β-sheets plates linked by π-stacking interactions and hydrogen bonding between side-chains (B). (C) Representation of the orthorhombic unit cell describing the peptide packing in the fibers.

Microscopy Imaging. Figure 3 shows AFM images for peptide films dried from solutions 4×10^{-4} wt % (below cac_1) ; 0.056 wt %, (marginally above the cac_2) ; and 0.5 wt % (well above cac_3). Topographic images reveal a clear relationship between morphology and concentration. In the most dilute regime, we observe small aggregates with heights of ~3 nm and lateral sizes ranging from ~15 nm to ~100 nm (lateral values probably overestimated by ~5 nm due to the finite size of the AFM tip[46]). The shape of these assemblies is irregular and elongated spheroids, possibly arising from association of two or more rounded units, are also observed. At an intermediate concentration, Figure 3B, the self-assembled nanostructure exhibits a dramatic change. A large number of spheroidal aggregates are observed with heights around 8 nm and lateral diameters around 20 nm. The formation of spheroidal aggregates has already been observed at the early stages of amyloid-fibrillization when small globular or ellipsoidal aggregates associate to form fibers.[46] Sinuous semiflexible fibrils are observed at high concentration (Figure 3C). A complex network of entangled fibers appears with widths ranging from ~20 to ~45 nm and heights ~10 nm. The results in Figure 3 clearly associate cac_1, cac_2, and cac_3 to the self-assembly in solution of three different species, as previously from the results displayed in Figures 1.

HRTEM was performed to assess the internal structure of the fibrils in Figure 3C in more detail. For this, samples were prepared from a solution with $[Arg\text{-}Phe]_4$ at 1.5 wt %. The corresponding images are displayed in Figure 3D−F, and they clearly reveal the presence of subunits forming the fibers. Specifically, we observe structures with sizes between 15 and 20 nm, formed from intertwined filaments with cross sections ~7 nm. In Figure 3D and E, these subfilaments are indicated by white arrows whereas fibers are highlighted by black arrows. Such a hierarchical process, where protofibrils entangle into larger filaments, apparently occurs down to quite small length scales as shown in Figure 3F. In this high-magnification image, we see thicker filaments formed by protofibrils as small as 2.5 nm wide.

X-ray Measurements. X-ray fiber diffraction was performed on stalks prepared from a concentrated sample containing the octapeptide at 5 wt % to probe the ordering of β-strands in the assemblies. A representative two-dimensional pattern from oriented fibers is exhibited in Figure 4A. This highly oriented pattern, corresponding to a very well ordered cross-β pattern, enables a detailed analysis of the fibril structure. Two meridional arcs are observed at d = 4.8 Å which are associated with the separation between adjacent peptide backbones organized into β-strands (position 6 in Figure 4A).[29] The pronounced localization of these reflections along the meridian indicates perpendicular orientation of strands with respect to the stalk axis and their sharpness points to a high degree of correlation between $[Arg\text{-}Phe]_4$ chains. Also along the vertical axis, we observe weak horizontal layer lines at $d \sim 9.6$ Å which corresponds to twice the β-strands separation and could indicate antiparallel organization of the chains.[47] Therefore, this distance is associated with the periodicity of strands with the same orientation along the structure. These meridional diffractions appear accompanied by a group of strong equatorial peaks at d = 27.4, 14.0, and 9.4 Å, indicating the presence of a lamellar phase along the fiber cross-section in agreement with previous molecular dynamic simulations.[15] A second group of equatorial reflections is found at 5.5, 4.8, and 4.0 Å. In addition to horizontal spots, spacing d = 5.5 Å and d = 4.0 Å are also found at off-axis positions. Analysis of these oriented reflections is more complex, but they indicate higher order-degree in the fibers and very efficient packing of peptide side-chains, possibly with helical twisting of β-sheets along the fiber axis.[48] To provide more detail on angular positions, a polar representation of the pattern is exhibited in Figure 4B, where azimuthal angles appear as a function of scattering vector. In Figure 4C, q-averaged profiles, integrated into thin slices around rings containing off-axis maxima, are shown. Peaks corresponding to d = 4.0 Å are observed at $\chi \sim \pm 36°$ (maxima are also found at $\chi \sim \pm 155°$; however, this region was not included in the polar representation because of beam stopper overlap). The peak at d = 5.5 Å is further from the azimuth and appears at $\chi \sim \pm 58°$ and $\chi \sim \pm 122°$.

The information in the XRD pattern allows to propose a structural model for $[Arg\text{-}Phe]_4$ fibers based on characteristic features of amyloid-like assemblies. We have indexed the

DOI: 10.1021/acs.langmuir.5b00253
Langmuir 2015, 31, 4513−4523

pattern according to an orthorhombic unit cell with lattice parameters a = 27.6 Å, b = 9.7 Å, and c = 9.6 Å. The outstanding equatorial reflections, marked by positions 1−3 in Figure 4A, have been assigned to Miller planes (100), (200), and (300), whereas the shallow meridional line at 9.6 Å and the intense arc at 4.8 Å have been attributed to planes (001) and (002), respectively. Finally, peaks at d = 5.5 Å and d = 4.0 Å have been indexed to planes (311) and (420), and simulations performed using the Fiber Diffraction Simulation module of CLEARER[26] (inset in Figure 4A) have properly predicted their off-axis positions. The lattice parameters arising from our structural model are fully compatible with major features typically observed in amyloid fibers.[48] For example, parameter a = 27.6 Å is assigned to the length of an extended octapeptide chain (~8 × 3.4 Å = 27.2 Å) and c = 9.6 Å is twice the separation between hydrogen bonded β-strands, consistent with antiparallel arrangement. The parameter b = 9.7 Å is compatible with the spacing between stacked β-sheets running parallel to the fiber axis.[49,50]

Figure 5 displays a tentative model for the internal structure of $[Arg\text{-}Phe]_4$ fibers, in keeping with the information extracted from the results displayed in Figures 3C−F and 4. The model in Figure 5 shows the formation of galleries hosting Phe or Arg layers, which are held together by strong π-stacking interactions and H-bonds between peptide backbones. We propose that the structure is stabilized due to the interplay of two complementary mechanisms. The first one is ascribed to the presence of counterions (namely, residual TFA arising from the synthesis procedure) screening electrostatic repulsions within arginine galleries. Similar phenomena have been recently reported to play a major role in the self-assembly and stabilization of peptide nanotubes built from cationic octapeptides.[51] The second one could be associated with a possible role of water molecules mediating H-bonding across the structure, in agreement with the strong H-bond donating behavior of arginine side-chains, consistent with previous molecular dynamic simulations.[15]" This arrangement, with hydrophobic galleries flanked by hydrophilic layers, is compatible with abundant $\pi-\pi$ interactions identified in our UV−vis data and is in good agreement with Pyr fluorescence, which has been found to be relatively low due to the presence of polar groups in the vicinity of chromophore species (Figure 1). Therefore, we propose that the inflection point in the Pyr fluorescence (Figure 1B) may be correlated to the appearance of the hydrophobic layers able to host nonpolar species. At lower concentrations, when the solution is populated by globular aggregates (Figure 3B), the system is less organized and presumably strong segregation of hydrophobic and hydrophilic sites is not present, accounting for the low value of the pyrene fluorescence emission.

SAXS provides convenient in situ methods to probe the internal structure of fibers. Solutions were prepared at four peptide concentrations: 0.05 wt %, close to the estimated cac_2; 0.1 wt %, 0.2 wt %, in the vicinities of cac_3; and 1 wt %, well above cac_3. In particular, a viscosity growth after a few days at room temperature of the more concentrated sample, suggested the formation of fibers. Samples studied by SAXS were investigated ~30 days after mixing. Figure 6 shows the SAXS curves measured at 0.05−1 wt % peptide and the overall results determined by model fitting analysis are summarized in Table 1. The shape of the curves clearly depends on peptide concentration; however, a common feature among them is the presence of two levels of structural organizations observed at

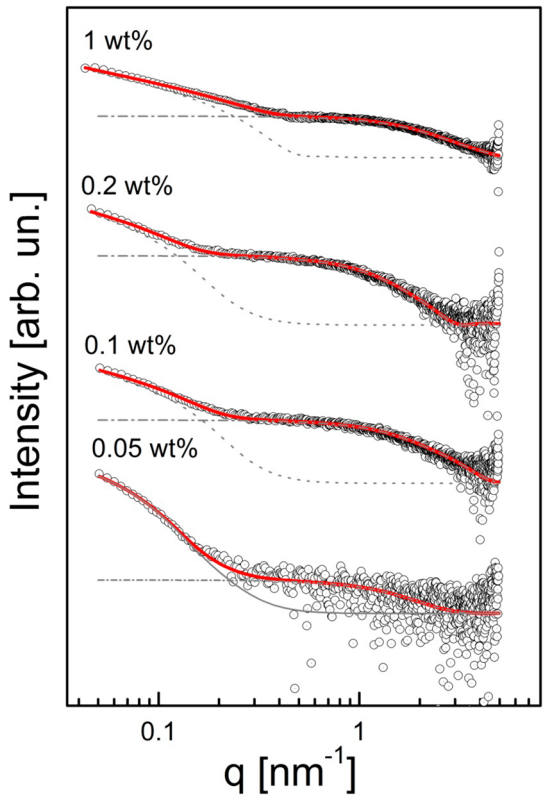

Figure 6. SAXS data from solutions containing $[Arg\text{-}Phe]_4$ peptides. Red lines correspond to fits performed using a combination of two form factors (see text for details). Solid gray line, ellipsoid form factor contribution; dotted gray line, long-cylinder contribution; and dashed-dotted gray line, short-cylinder contribution.

intermediate q-values. The SAXS curves are characterized by a smooth descent and to describe this high-angle region we have used a Porod cylinder form factor[52] plus a flat background (see eqs SI2 and SI3 in the Supporting Information). Our results show that contributions from these small particles are well-described by short cylinders with radii between R = 0.6 and 1.1 nm, and lengths between L = 2.6 and 4.5 nm. We ascribe this component to the presence of small oligomers hosting just a few $[Arg\text{-}Phe]_4$ strands. The volume of these cylindrical aggregates ranges from ~3 to ~17 nm^3 being able to accommodate from ~2 to ~11 monomers (octapeptide volume ~ 1.5 nm^3). SAXS is a powerful method providing structural information on amyloid oligomers;[53,54] however, accurate analysis is complex[2] since they are present at low concentration and have low molecular weight and many species may coexist in solution.

The most dilute sample, 0.05 wt %, exhibits a profile which contrasts with its more concentrated counterparts. The low-q region of this sample is characterized by a remarkable curvature and data from this domain have been properly fitted using a form factor for polydisperse ellipsoids (see eq SI4).[52] Our results have led to average prolate-shaped particles with semiprincipal axis of 43.4 ± 31.7 nm and radii R = 12.3 ± 8.9 nm, where uncertainty has been obtained from the standard deviation of a Gaussian distribution. These results agree with AFM images from samples at this same concentration, where aggregates of spheroidal particles with diameters averaging ~20 nm have been found (see Figure 3B). The presence of similar structures, both in size and shape, has been observed in the

DOI: 10.1021/acs.langmuir.5b00253
Langmuir 2015, 31, 4513−4523

Table 1. Parameters Obtained from Model Fitting of SAXS Data

		short cyl form factor		long cyl form factor[a]	ellipsoid form factor	
sample (wt %)	contribution	R (nm)	L (nm)	$R \pm$ SD (nm)	$R \pm$ SD (nm)	$\nu R \pm$ SD (nm)
0.05	oligomers	1.0	3.2			
	aggregates				12.3 ± 8.9	43.4 ± 31.7
0.1	oligomers	0.7	3.3			
	fibers			7.0 ± 4.9		
0.2	oligomers	1.1	4.5			
	fibers			8.0 ± 6.7		
1	oligomers	0.6	2.6			
	fibers			6.5 ± 1.1		

[a]Cylinder length fixed at L = 500 nm and scattering length density fixed at η = 1.

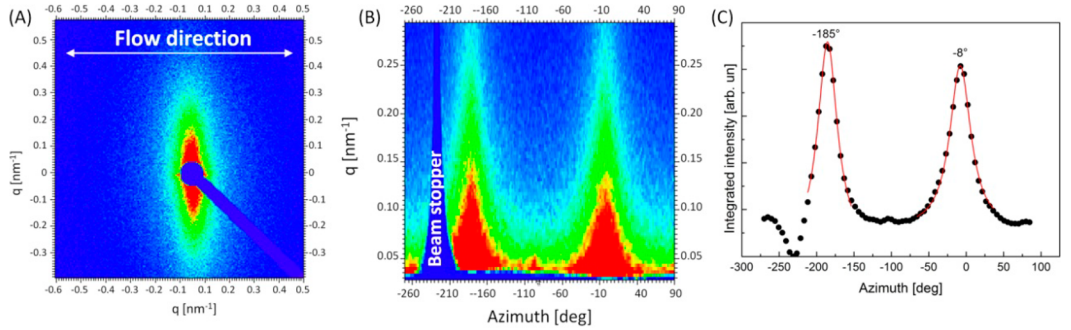

Figure 7. SAXS data from aged [Arg-Phe]$_4$ solution under linear flow. (A) 2D pattern exhibiting strong anisotropy along direction perpendicular to shear. (B) Polar representation of pattern exhibited in (A) and corresponding q-averaged azimuthal intensities.

context of amyloid formation where these aggregates are frequently described as "seeds" in the pathway toward the growth of fibers.[2,47,53] The high degree of dispersity in the radii in our solution data could be ascribed to the proximity to a critical regime, where association and dissociation between aggregates strongly affect the dynamic equilibrium and presumably generates size polydispersity.

For the more concentrated samples, the low-q regions in the SAXS profiles do not have a curved shape being rather typified by a linear profile scaling with q^{-1}. This characteristic indicates that this domain is dominated by a cylinder form factor, in accordance with fibrillar structures in solution. To describe these profiles, we have used Porod's approximation for long cylinders[52] together with a Gaussian distribution to account for polydispersity in fiber radii. The length of cylinders was fixed at L = 500 nm in agreement with long persistence lengths indicated by TEM images and, since $L \gg R$, this parameter simply behaved as a scaling factor. The scattering length density was arbitrarily fixed at η = 1 and thus only four parameters (radius, standard deviation, a scaling constant and a background constant) were left free to adjust. Our fitting procedures yielded R = 7.0 ± 4.9 nm, R = 8.0 ± 6.7 nm, and R = 6.5 ± 1.1 nm, respectively, for samples with concentrations 0.1, 0.2, and 1 wt %. It should be noted that, although the concentration 0.1 wt % is marginally below cac$_3$, data could not be properly described by sphere form factors likely associated with globular aggregates. We suspect that this could be related to the fact of SAXS measurements had been performed ∼4 weeks after sample preparation which could imply some time-dependent evolution of the assemblies as found in our aged sample discussed below. We observe that the in situ measurements agree with images from AFM and TEM; however, an interesting feature arising from these assays is that fibers exhibit high polydispersity in solution at lower concentrations. The fibers found here show a wide range of sizes in the mixture, which may be due to their assembly from smaller protofilaments, suggested by the modeling of the XRD data discussed above. Considering averages and standard deviations, fibers have minimum radius of ∼1.3 nm and a maximum ∼15 nm. The lowest values could be assigned to the size of a protofilament formed by a pair of twisted β-sheets, whereas the largest one is compatible with a pair of bundled fibers such those ones observed in microscopy assays. The mature fibers have radii ∼ 7.0 nm and are made up by five or six intertwined protofilaments. In this case, the fibers investigated here exhibit unequivocal features of amyloid-like structures across the mesoscale, from the supramolecular level, where cross-β strands assembled into β-sheets, up to nanometer dimensions where intertwined protofilaments form the fibers.[55]

Upon increasing concentration, SAXS shows that the fibril radius polydispersity decreases sharply. In this case, the mixture is considerably above cac and thus far from the critical regime. In this scenario, equilibrium between fibers and oligomeric species is shifted favoring fibrillization and this may explain the reduced polydispersity. In fact, concomitantly with a decrease in polydispersity of fibrillar component, we observe that the short-cylinder contribution used to describe the high-angle region of the SAXS curves exhibits the lowest volume among investigated samples corresponding approximately to dimers in solution.

We have also observed formation of weak gel solutions upon aging under refrigerated conditions. In addition to samples discussed above, a 1 wt % formulation was examined ∼120 days after preparation, when it exhibited higher viscosity and appreciable adhesion to walls of the vial. To provide some insight on this state, we performed SAXS under flow using rate of Q = 8.3 μL·s^{-1} across a 1 mm wide capillary. These conditions imply a Newtonian shear rate at the wall of $\dot{\gamma}$ =

DOI: 10.1021/acs.langmuir.5b00253
Langmuir 2015, 31, 4513−4523

$32Q/\pi R^3 = 85\ s^{-1}$. A representative 2D pattern obtained under these conditions is shown in Figure 7A, and it clearly exhibits high anisotropy along the vertical axis which is indicates alignment along flow direction (horizontal). In Figure 7B, we show the polar representation of the pattern, confirming that the intensity maxima are highly concentrated around the meridional axes and the corresponding q-integrated profile, Figure 7C, shows peaks at −8° and −185°. A quantitative estimation on orientation could be calculated through the orientational order parameter given by[56]

$$F = \frac{(3\cos^2\chi - 1)}{2} \tag{2a}$$

$$\cos^2\chi = \frac{\int_0^\pi I(q,\chi)\cos^2\chi \sin\chi \, d\chi}{\int_0^\pi I(q,\chi)\sin\chi \, d\chi} \tag{2b}$$

where $I(q,\chi)$ is the q-integrated intensity at a given azimuthal angle χ. From eq 2, we obtained an order parameter $F \sim 0.2$ which denotes high orientation upon relatively gentle shear. We suspect that this state of the mixture arises from a high correlation between fibers, possibly due to entanglements formed upon aging. In fact, such anisotropy in the scattering profile is not observed at early stages when fibers are uncorrelated and likely do not form networks in solution. These findings indicate that these $[Arg\text{-}Phe]_4$ fibrils could be used for preparing self-sustained matrices and possibly designing hydrogel materials in the future. This could be particularly attractive for providing an arginine-rich medium either to host molecular cargoes[57,58] or to investigate specific reactions, for example, nitric oxide catalysis,[59,60] involving this amino acid in a biomimetic environment.

CONCLUSIONS

We have found that an alternating arginine/phenylalanine octapeptide forms amyloid-type β-sheet rich fibrils and other amyloid-like analogs along its self-assembly pathway. Critical aggregation concentrations obtained from complementary fluorescence and absorbance spectroscopy provided a detailed picture of the multistep aggregation process. Particularly, our data suggest the formation oligomeric species at concentrations as low as ∼0.001 wt % and the spontaneous appearance of spheroidal, β-sheet rich, aggregates at ∼0.035 wt %. At higher concentrations, above a critical value estimated at 0.17 wt %, long fibers appear in solution. The secondary structure is predominantly β-sheets as revealed by FTIR and CD spectroscopy. TEM shows that the fibrils are composed of intertwined protofilaments. Fiber diffraction revealed high level of crystalline symmetry with peptides organized into an orthorhombic unit cell with lattice parameters a = 27.4 Å, b = 9.7 Å, and c = 9.6 Å. The XRD pattern unequivocally confirms a cross-β conformation with antiparallel strands separated by 4.8 Å perpendicularly arranged into β-sheets running parallel to the fiber long axis. In this configuration, our model suggests the presence of galleries between stacked β-sheets comprising phenylalanine or arginine side-chains which are kept together by strong π-stacking interactions and H-bonds. Different numbers of interlaced fibrils lead to bundles of fibrils with polydispersity in diameter. This conclusion was clearly supported by the SAXS data, which shows the presence of size distributions accounting for different size populations in solutions. In addition to fibers, the SAXS data indicate the formation of oligomeric aggregates in solution, even above the cac. These assemblies were modeled using approximations to short cylindrical shapes and rough estimations from their sizes and volumes allowed us estimate that there may be a significant contribution from monomers close to the cac, with dimers/trimers and higher aggregates forming at higher concentrations. Also, we found that upon aging the fibers form interconnected networks able to align under gentle shearing. Our results show that the $[Arg\text{-}Phe]_4$ octapeptide is a useful model peptide, with a highly simplified sequence, incorporating dual functionality from aromatic and cationic residues, that exhibits all the characteristics associated with amyloid fibers.

ASSOCIATED CONTENT

Supporting Information

SAXS modeling and equations. This material is available free of charge via the Internet at http://pubs.acs.org.

AUTHOR INFORMATION

Corresponding Authors

*E-mail: ersilva@ufabc.edu.br. Tel.: +55 11 4996 0035.
*E-mail: wendel.alves@ufabc.edu.br. Tel.: +55 11 4996 0193. Fax: +55 11 4996 3166.

Notes

The authors declare no competing financial interest.

ACKNOWLEDGMENTS

C.C.D. thanks UFABC for fellowships. E.R.S., M.S.L., and W.A.A. acknowledge FAPESP (postdoc internship abroad 2014/03514-8, Ph.D. fellowship 2012/15481-1, and regular support 2013/12997-0). I.W.H. was supported by a Royal Society-Wolfson Research Merit Award. C.L.P.O. is supported by CNPq and INCT-FCx. We are grateful for the SRCD beamtime awarded at the B23 beamline (Diamond Light Source, UK; Project Number SM10083-1) and to R. Hussain for help during SRCD experiments. We would like to acknowledge B. Calisto and A. Round for support during beamtimes at BM29 (ESRF, Grenoble, Project Numbers MX 1620 and MX1666). LNano staff (C. Costa, E. Lanzoni, R. Portugal, and A. Cassago) are acknowledged for helpful instructions during AFM and HR-TEM assays (Proposals AFM2-16867 and TEM-MSC 16618). B. Ferrante (UFABC) is acknowledged for aid during peptide cleavage. T. Germano, D. Reis (at USP), A. Dehsorkhi, and N. Spencer (at UoR) are recognized for helping with exploratory lab SAXS assays and fiber diffraction experiments. We thank Prof. Louise Serpell (Univ. Sussex) for providing a copy of the program CLEARER used for unit cell optimizations in our XRD analyses. P. Oseliero (IFUSP) and T. Manieri (UFABC) are acknowledged for helpful discussions on eq 1 and support during lab-based CD assays.

REFERENCES

(1) Hamley, I. W. Peptide Nanotubes. *Angew. Chem., Int. Ed.* **2014**, *53*, 6866−6881.
(2) Hamley, I. W. The Amyloid Beta Peptide: A Chemist's Perspective. Role in Alzheimer's and Fibrillization. *Chem. Rev.* **2012**, *112*, 5147−5192.
(3) Selkoe, D. J. Alzheimer's Disease: Genes, Proteins, and Therapy. *Physiol. Rev.* **2001**, *81*, 741−766.
(4) Chiti, F.; Dobson, C. M. Protein Misfolding, Functional Amyloid, and Human Disease. *Annu. Rev. Biochem.* **2006**, *75*, 333−366.

DOI: 10.1021/acs.langmuir.5b00253
Langmuir 2015, 31, 4513−4523

(5) Hamley, I. W. Peptide Fibrillization. *Angew. Chem., Int. Ed.* **2007**, *46*, 8128−8147.
(6) Tjernberg, L. O.; Callaway, D. J. E.; Tjernberg, A.; Hahne, S.; Lilliehook, C.; Terenius, L.; Thyberg, J.; Nordstedt, C. A Molecular Model of Alzheimer Amyloid Beta-Peptide Fibril Formation. *J. Biol. Chem.* **1999**, *274*, 12619−12625.
(7) Tjernberg, L. O.; Lilliehook, C.; Callaway, D. J. E.; Naslund, J.; Hahne, S.; Thyberg, J.; Terenius, L.; Nordstedt, C. Controlling Amyloid Beta-Peptide Fibril Formation with Protease-Stable Ligands. *J. Biol. Chem.* **1997**, *272*, 12601−12605.
(8) Krysmann, M. J.; Castelletto, V.; Kelarakis, A.; Hamley, I. W.; Hule, R. A.; Pochan, D. J. Self-Assembly and Hydrogelation of an Amyloid Peptide Fragment. *Biochemistry* **2008**, *47*, 4597−4605.
(9) Tjernberg, L. O.; Pramanik, A.; Bjorling, S.; Thyberg, P.; Thyberg, J.; Nordstedt, C.; Berndt, K. D.; Terenius, L.; Rigler, R. Amyloid Beta-Peptide Polymerization Studied Using Fluorescence Correlation Spectroscopy. *Chem. Biol.* **1999**, *6*, 53−62.
(10) Tjernberg, L. O.; Naslund, J.; Lindqvist, F.; Johansson, J.; Karlstrom, A. R.; Thyberg, J.; Terenius, L.; Nordstedt, C. Arrest of Beta-Amyloid Fibril Formation by a Pentapeptide Ligand. *J. Biol. Chem.* **1996**, *271*, 8545−8548.
(11) Naslund, J.; Schierhorn, A.; Hellman, U.; Lannfelt, L.; Roses, A. D.; Tjernberg, L. O.; Silberring, J.; Gandy, S. E.; Winblad, B.; Greengard, P.; Nordstedt, C.; Terenius, L. Relative Abundance of Alzheimer A-Beta Amyloid Peptide Variants in Alzheimer-Disease and Normal Aging. *Proc. Natl. Acad. Sci. U. S. A.* **1994**, *91*, 8378−8382.
(12) Gazit, E. A Possible Role for Pi-Stacking in the Self-Assembly of Amyloid Fibrils. *FASEB J.* **2002**, *16*, 77−83.
(13) Serpell, L. Amyloid Structure. *Essays Biochem.* **2014**, *56*, 1−10.
(14) Jahn, T. R.; Makin, O. S.; Morris, K. L.; Marshall, K. E.; Tian, P.; Sikorski, P.; Serpell, L. C. The Common Architecture of Cross-beta Amyloid. *J. Mol. Biol.* **2010**, *395*, 717−727.
(15) Liberato, M. S.; Kogikoski, S.; da Silva, E. R.; Silva, R. H.; Oliveira, V. X.; Scott, L. P.; Ando, R. A.; Alves, W. A.; Coutinho-Neto, M. D. Self-Assembly of Arg-Phe Nanostructures via the Solid-Vapor Phase Method. *J. Phys. Chem. B* **2013**, *117*, 733−740.
(16) Zhang, S. G.; Lockshin, C.; Cook, R.; Rich, A. Unusually Stable Beta-Sheet Formation in an Ionic Self-Complementary Oligopeptide. *Biopolymers* **1994**, *34*, 663−672.
(17) Zhang, S. Emerging Biological Materials Through Molecular Self-Assembly. *Biotechnol. Adv.* **2002**, *20*, 321−339.
(18) Maslovskis, A.; Guilbaud, J. B.; Grillo, I.; Hodson, N.; Miller, A. F.; Saiani, A. Self-Assembling Peptide/Thermoresponsive Polymer Composite Hydrogels: Effect of Peptide-Polymer Interactions on Hydrogel Properties. *Langmuir* **2014**, *30*, 10471−10480.
(19) Mujeeb, A.; Miller, A. F.; Saiani, A.; Gough, J. E. Self-Assembled Octapeptide Scaffolds for *in vitro* Chondrocyte Culture. *Acta Biomater.* **2013**, *9*, 4609−4617.
(20) Boothroyd, S.; Saiani, A.; Miller, A. F. Formation of Mixed Ionic Complementary Peptide Fibrils. *Macromol. Symp.* **2008**, *273*, 139−145.
(21) Guilbaud, J. B.; Vey, E.; Boothroyd, S.; Smith, A. M.; Ulijn, R. V.; Saiani, A.; Miller, A. F. Enzymatic Catalyzed Synthesis and Triggered Gelation of Ionic Peptides. *Langmuir* **2010**, *26*, 11297−11303.
(22) Shimoni, L.; Glusker, J. P. Hydrogen-Bonding Motifs of Protein Side-Chains − Descriptions of Binding of Arginine and Amide Groups. *Protein Sci.* **1995**, *4*, 65−74.
(23) Gallivan, J. P.; Dougherty, D. A. Cation-pi Interactions in Structural Biology. *Proc. Natl. Acad. Sci. U. S. A.* **1999**, *96*, 9459−64.
(24) Wojdyr, M. Fityk: a general-purpose peak fitting program. *J. Appl. Crystallogr.* **2010**, *43*, 1126−1128.
(25) Necas, D.; Klapetek, P. Gwyddion: An Open-Source Software for SPM Data Analysis. *Cent. Eur. J. Phys.* **2012**, *10*, 181−188.
(26) Makin, O. S.; Sikorski, P.; Serpell, L. C. CLEARER: a New Tool for the Analysis of X-Ray Fibre Diffraction Patterns and Diffraction Simulation from Atomic Structural Models. *J. Appl. Crystallogr.* **2007**, *40*, 966−972.
(27) Bressler, J. K. a. I. *SASfit for Fitting Small-Angle Scattering Curves*, 0.93.5; Paul Scherrer Institute: Villigen, 2011.
(28) Nilsson, M. R. Techniques to Study Amyloid Fibril Formation *in vitro*. *Methods* **2004**, *34*, 151−160.
(29) Castelletto, V.; Gouveia, R. M.; Connon, C. J.; Hamley, I. W. New RGD-Peptide Amphiphile Mixtures Containing a Negatively Charged Diluent. *Faraday Discuss.* **2013**, *166*, 381−397.
(30) Winnik, F. M. Photophysics of Preassociated Pyrenes in Aqueous Polymer-Solutions and in Other Organized Media. *Chem. Rev.* **1993**, *93*, 587−614.
(31) Hamley, I. W.; Dehsorkhi, A.; Castelletto, V. Coassembly in Binary Mixtures of Peptide Amphiphiles Containing Oppositely Charged Residues. *Langmuir* **2013**, *29*, 5050−5059.
(32) Karabacak, M.; Cinar, M.; Kurt, M.; Babu, P. C.; Sundaraganesan, N. Experimental and Theoretical FTIR and FT-Raman Spectroscopic Analysis of 1-Pyrenecarboxylic Acid. *Spectrochim. Acta, Part A* **2013**, *114*, 509−519.
(33) Piao, L.; Liu, Q.; Li, Y.; Wang, C. Adsorption of L-Phenylalanine on Single-Walled Carbon Nanotubes. *J. Phys. Chem. C* **2008**, *112*, 2857−2863.
(34) Shimizu, S.; Pires, P. A. R.; El Seoud, O. A. Thermodynamics of Micellization of Benzyl(2-acylaminoethyl)Dimethylammonium Chloride Surfactants in Aqueous Solutions: A Conductivity and Titration Calorimetry Study. *Langmuir* **2004**, *20*, 9551−9559.
(35) Kiraly, Z.; Dekany, I. A Thermometric Titration Study on the Micelle Formation of Sodium Decyl Sulfate in Water. *J. Colloid Interface Sci.* **2001**, *242*, 214−219.
(36) Byler, D. M.; Susi, H. Examination of the Secondary Structure of Proteins by Deconvoluted FTIR Spectra. *Biopolymers* **1986**, *25*, 469−487.
(37) Moran, S. D.; Zanni, M. T. How to Get Insight into Amyloid Structure and Formation from Infrared Spectroscopy. *J. Phys. Chem. Lett.* **2014**, *5*, 1984−1993.
(38) Eker, F.; Griebenow, K.; Schweitzer-Stenner, R. A Beta(1−28) Fragment of the Amyloid Peptide Predominantly Adopts a Polyproline II Conformation in an Acidic Solution. *Biochemistry* **2004**, *43*, 6893−6898.
(39) Hong, J.; Wert, J.; Asher, S. A. UV Resonance Raman and DFT Studies of Arginine Side Chains in Peptides: Insights into Arginine Hydration. *J. Phys. Chem. B* **2013**, *117*, 7145−7156.
(40) Barth, A. The Infrared Absorption of Amino Acid Side Chains. *Prog. Biophys. Mol. Biol.* **2000**, *74*, 141−173.
(41) Frey, B. L.; Corn, R. M. Covalent Attachment and Derivatization of Poly(L-Lysine) Monolayers on Gold Surfaces as Characterized by Polarization-Modulation FT-IR Spectroscopy. *Anal. Chem.* **1996**, *68*, 3187−3193.
(42) Nordén, B.; Rodger, A.; Dafforn, T. *Linear dichroism and circular dichroism: a textbook on polarized-light spectroscopy*; Royal Society of Chemistry: Cambridge, 2010; p 293.
(43) Bulheller, B. M.; Rodger, A.; Hirst, J. D. Circular and Linear Dichroism of Proteins. *Phys. Chem. Chem. Phys.* **2007**, *9*, 2020−2035.
(44) Woody, R. W. Aromatic Side-Chain Contributions to the Far Ultraviolet Circular Dichroism of Peptides and Proteins. *Biopolymers* **1978**, *17*, 1451−1467.
(45) Brahms, S.; Brahms, J.; Spach, G.; Brack, A. Identification of *β*,*β*-Turns and Unordered Conformations in Polypeptide Chains by Vacuum Ultraviolet. *Proc. Natl. Acad. Sci. U.S.A.* **1977**, *74*, 3208−3212.
(46) Kowalewski, T.; Holtzman, D. M. In situ Atomic Force Microscopy Study of Alzheimer's Beta-Amyloid Peptide on Different Substrates: New Insights into Mechanism of Beta-Sheet Formation. *Proc. Natl. Acad. Sci. U. S. A.* **1999**, *96*, 3688−3693.
(47) Serpell, L. C. Alzheimer's Amyloid Fibrils: Structure and Assembly. *Biochim. Biophys. Acta, Mol. Basis Dis.* **2000**, *1502*, 16−30.
(48) Morris, K. L.; Zibaee, S.; Chen, L.; Goedert, M.; Sikorski, P.; Serpell, L. C. The Structure of Cross-beta Tapes and Tubes Formed by an Octapeptide, alpha S beta 1. *Angew. Chem., Int. Ed.* **2013**, *52*, 2279−2283.
(49) Rosler, A.; Klok, H. A.; Hamley, I. W.; Castelletto, V.; Mykhaylyk, O. O. Nanoscale Structure of Poly(ethylene glycol)

DOI: 10.1021/acs.langmuir.5b00253
Langmuir 2015, 31, 4513−4523

Hybrid Block Copolymers Containing Amphiphilic Beta-Strand Peptide Sequences. *Biomacromolecules* **2003**, *4*, 859−863.
(50) Haris, P. I.; Chapman, D. The Conformational Analysis of Peptides Using Fourier Transform IR Spectroscopy. *Biopolymers* **1995**, *37*, 251−263.
(51) Gobeaux, F.; Fay, N.; Tarabout, C.; Meriadec, C.; Meneau, F.; Ligeti, M.; Buisson, D.-A.; Cintrat, J.-C.; Nguyen, K. M. H.; Perrin, L.; Valery, C.; Artzner, F.; Paternostre, M. Structural Role of Counterions Adsorbed on Self-Assembled Peptide Nanotubes. *J. Am. Chem. Soc.* **2012**, *134*, 723−733.
(52) Pedersen, J. S. Analysis of Small-Angle Scattering Data from Colloids and Polymer Solutions: Modeling and Least-Squares Fitting. *Adv. Colloid Interface Sci.* **1997**, *70*, 171−210.
(53) Vestergaard, B.; Groenning, M.; Roessle, M.; Kastrup, J. S.; van de Weert, M.; Flink, J. M.; Frokjaer, S.; Gajhede, M.; Svergun, D. I. A Helical Structural Nucleus is the Primary Elongating Unit of Insulin Amyloid Fibrils. *PLoS Biol.* **2007**, *5*, e134.
(54) Oliveira, C. L. P.; Behrens, M. A.; Pedersen, J. S.; Erlacher, K.; Otzen, D.; Pedersen, J. S. A SAXS Study of Glucagon Fibrillation. *J. Mol. Biol.* **2009**, *387*, 147−161.
(55) Malinchik, S. B.; Inouye, H.; Szumowski, K. E.; Kirschner, D. A. Structural Analysis of Alzheimer's Beta(1−40) Amyloid: Protofilament Assembly of Tubular Fibrils. *Biophys. J.* **1998**, *74*, 537−545.
(56) Alexander, L. E. *X-ray diffraction methods in polymer science*; Wiley-Interscience: New York, 1969; p 582.
(57) Zhang, Z.; Lai, Y.; Yu, L.; Ding, J. Effects of Immobilizing Sites of RGD Peptides in Amphiphilic Block Copolymers on Efficacy of Cell Adhesion. *Biomaterials* **2010**, *31*, 7873−7882.
(58) Castelletto, V.; Gouveia, R. M.; Connon, C. J.; Hamley, I. W.; Seitsonen, J.; Nykanen, A.; Ruokolainen, J. Alanine-Rich Amphiphilic Peptide Containing the RGD Cell Adhesion Motif: a Coating Material for Human Fibroblast Attachment and Culture. *Biomater. Sci.* **2014**, *2*, 362−369.
(59) He, M. Y.; Potuck, A.; Zhang, Y.; Chu, C. C. Arginine-based polyester amide/polysaccharide hydrogels and their biological response. *Acta Biomater.* **2014**, *10*, 2482−2494.
(60) Marletta, M. A. Nitric-Oxide Synthase - Aspects Concening Structure and Catalysis. *Cell* **1994**, *78*, 927−930.

DOI: 10.1021/acs.langmuir.5b00253
Langmuir 2015, 31, 4513−4523